ACS OMEGA

http://pubs.acs.org/journal/acsodf

Article

# Biodiesel Production from Waste Cooking Oil via β-Zeolite-Supported Sulfated Metal Oxide Catalyst Systems

Basiru O. Yusuf, Sulayman A. Oladepo,* and Saheed A. Ganiyu

Cite This: *ACS Omega* 2023, 8, 23720−23732

Read Online

ACCESS | Metrics & More | Article Recommendations | Supporting Information

**ABSTRACT:** Waste cooking oil (WCO) is a readily available and cheap feedstock for biodiesel production. However, WCO contains high levels of free fatty acids (FFAs), which negatively impact the biodiesel yield if homogeneous catalysts are used. Heterogeneous solid acid catalysts are preferred for low-cost feedstocks because the catalysts are highly insensitive to high levels of FFA in the feedstock. Therefore, in the present study, we synthesized and evaluated different solid catalysts, pure β-zeolite, ZnO-β-zeolite, and $SO_4^{2-}$/ZnO-β-zeolite for the production of biodiesel using WCO as feedstock. The synthesized catalysts were characterized by Fourier transform infrared spectroscopy (FTIR), pyridine-FTIR, $N_2$ adsorption−desorption, X-ray diffraction, thermogravimetric analysis, and scanning electron microscopy, while the biodiesel product was analyzed using nuclear magnetic resonance ($^1$H and $^{13}$C NMR) and gas chromatography−mass spectroscopy. The results revealed that the $SO_4^{2-}$/ZnO-β-zeolite catalyst showed excellent catalytic performance for simultaneous transesterification and esterification of WCO, with a higher percentage conversion than the ZnO-β-zeolite and pure β-zeolite catalyst, due to the large pore size and high acidity. The $SO_4^{2-}$/ZnO-β-zeolite catalyst exhibits 6.5 nm pore size, a total pore volume of 0.17 cm$^3$/g, and high surface area of 250.26 m$^2$/g. Experimental parameters such as catalyst loading, methanol:oil molar ratio, temperature, and reaction time were varied in order to establish the optimal parameters. The highest WCO conversion of 96.9% was obtained using the $SO_4^{2-}$/ZnO-β-zeolite catalyst under an optimum reaction condition of 3.0 wt % catalyst loading, 200 °C reaction temperature, and 15:1 molar ratio of methanol to oil in 8 h reaction time. The WCO-derived biodiesel properties conform to the ASTM6751 standard specification. Our investigation of its kinetics revealed that the reaction follows a pseudo first-order kinetic model, with an activation energy ($E_a$) of 38.58 kJ/mol. Moreover, the stability and reusability of the catalysts were evaluated, and it was found that the $SO_4^{2-}$/ZnO-β-zeolite catalyst exhibited good stability, giving a biodiesel conversion of over 80% after three synthesis cycles.

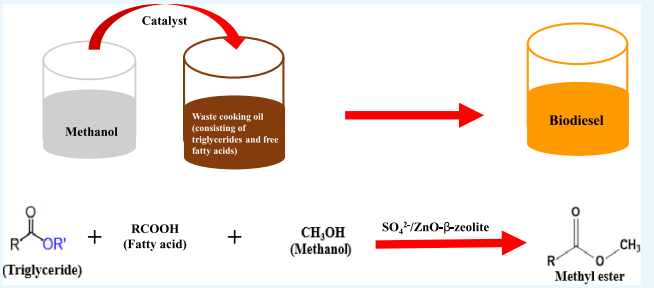


## 1. INTRODUCTION

Fossil fuels have been major fuel sources for domestic and industrial uses, and they meet the majority of the world's energy demands and use in petrochemicals.[1,2] Nevertheless, fossil fuels are linked to major environmental issues such as greenhouse gas emissions, air pollution, oil spillage, and degradation of aquatic and arable land.[3−5] Biofuels have a high priority among fuel alternatives because of their renewable nature. Biodiesel is regarded as the most promising renewable fuel among the various biofuels, presumably owing to its nontoxic, biodegradable, and renewable nature, as well as its low carbon monoxide and sulfur emissions during combustion.[6] Biodiesel is produced by either transesterification of triglycerides or esterification of free fatty acids (FFAs) with methanol using a suitable catalyst, leading to fatty acid methyl ester (biodiesel) and glycerol.[7] Vegetable oil-based biodiesel typically costs more than 0.50 USD L$^{-1}$,[8,9] and depending on the feedstock oils, the price can be about 1.5 times that of fossil-based diesel.[8] Use of cheap starting materials like non-edible oil and waste cooking oil (WCO) rather than fresh vegetable oils and the development of highly active, cost-effective, and easily recyclable catalysts can lower the production costs of biodiesel.[8,9] Moreover, using WCO offers three possible advantages: environmental sustainability, waste management, and good economics. Detailed economic analyses have shown that use of WCO is more economically feasible and profitable because of the lowest manufacturing cost, attractive rate of return, and reduction in selling prices.[10,11]

Owing to the high FFAs and water content in WCO, using a homogeneous base catalyst will result in saponification, which will cause significant difficulties with product separation and eventually, a significant reduction in biodiesel yield. When using feedstocks that contain a high level of FFAs, a two-step

Received: March 20, 2023
Accepted: June 7, 2023
Published: June 19, 2023

approach is typically employed.[12,13] Pre-esterification of FFAs with alcohol is the first step, in which the FFAs are catalyzed using liquid acids (liquid acid catalysis, which reduces the FFAs content in oil by more than 99%). In the second step, the products from the first step are converted into biodiesel and glycerol by base-catalyzed transesterification. Unlike base catalysts, FFAs have no effect on homogenous acid catalysts, and homogenous acid catalysts are capable of catalyzing both transesterification and esterification simultaneously.[14] Nevertheless, separation and regeneration of the catalyst, corrosion-related problems, and serious environmental issues limit the utilization of homogeneous acid catalysts. The use of heterogeneous catalysts to produce biodiesel is gaining popularity due to the fact that they are recyclable and offer a simple catalyst removal step.[15] Heterogeneous acid catalysts may be less active but they are more stable than heterogeneous base catalysts, allowing them to be employed for feedstocks containing a high quantity of FFAs without catalyst deactivation.[16]

Many scientists have made substantial progress toward producing biodiesel through solid acid catalysts.[17] Heterogeneous acid catalysts employed for triglyceride transesterification, including zeolite, Amberlyst-15, and sulfated tin oxide ($SO_4^{2-}/SnO_2$), exhibited high catalytic activity.[18] Solid acid catalysts have also been used to esterify FFAs.[19] Incorporation of the sulfate group into metal oxides primarily improves acidity without compromising the catalytic activity.[19−21] Sulfated titanium oxide ($SO_4^{2-}/TiO_2$), ion-exchange resin, sulfated zirconium oxide ($SO_4^{2-}/ZrO_2$), and sulfated tin oxide are some examples of typical catalysts with high catalytic activity.[19−21] When utilized to catalyze both transesterification and esterification simultaneously, some of these heterogeneous acid catalysts, like sulfated titanium oxide, demonstrated remarkable catalytic activity and stability.[21,22]

Latest developments in solid acid catalysts for biodiesel production are predicated on the fact that such catalysts have better tolerance for high contents of FFA and water present in low quality oils such as WCO. Solid acid catalysts are so FFA-tolerant that several researchers have demonstrated their suitability for esterification of fatty acids.[23,24] In a recent report, Zhang and Xie synthesized ZrMo oxides catalyst supported on hierarchical porous structure made of polystyrene and used the resulting catalyst system for biodiesel production from acidic oils.[23] The catalyst is recyclable and gave 93.8% oil conversion. The authors claimed that incorporation of transition metal oxides into porous support materials is a viable way to significantly increase the catalytic surface area, heterogeneity, and catalytic performance.[23] In a similar vein, Lin and co-workers used polymerization and ion-exchange to prepare a series of poly(divinylbenzene) polymer-based solid acid catalysts using various p-styrene sulfonate/divinylbenzene loading ratios. The resulting catalyst was used for the transesterification of waste palmitic oils, giving a biodiesel yield of 83.3%.[24] This work shows that their acidic catalyst can efficiently convert waste oils containing FFA from triglycerides and FFA to biodiesel.[24]

Several research groups have also reported the use of heterogeneous nanocatalysts for biodiesel production, including zinc oxide, calcium oxide, magnesium oxide, zirconium oxide, iron oxide, and cobalt oxide nanocatalysts.[25−28] For instance, Saravanan et al. used a solvent-free approach to prepare 11 nm sulfated zirconia nanoparticles by the precipitation technique and then used them as nanocatalysts for transesterification of palmitic acid, which gives a 90% yield.[27] Other types of solid acid catalysts have also been used for biodiesel production.[29,30] For example, Brønsted acidic ionic liquids have also been exploited for the catalytic transesterification of coconut oil.[29] A biodiesel yield of 98.3% was obtained, and there was no significant reduction in catalytic activity even after 5 reaction cycles.

Perhaps in line with the claim of Zhang and Xie that incorporation of solid acid catalysts in porous support materials will increase their surface area and catalytic performance, several researchers have harnessed metal−organic frameworks (MOFs) as a catalyst support.[31−34] Using zeolitic imidazolate framework (ZIF-90), Mao and co-workers modified the MOF with sulfamic acid, thereby increasing the number of Brønsted and Lewis acid sites of the framework. They used the catalyst for microbial biodiesel production and obtained 98.3% conversion.[31] Similarly, a novel bismuth-based MOF impregnated with phosphomolybdic acid (PMA@Bi-BTC) was used by Zhang et al. for the conversion of oleic acid to biodiesel.[32] They reported that the catalyst gave a conversion of 92.5%, which was attributed to textural property of the catalyst, the presence of more acid sites, and the synergistic catalytic effects between the duo of phosphomolybdic acid and Bi-BTC.[32] An efficient and stable heterogeneous acid catalyst has also been synthesized by impregnation method, combining UiO-66 MOFs and ammonium sulfate.[34] The resulting solid acid catalyst was put through a two-stage calcination process under a nitrogen atmosphere in order to enhance the catalyst stability, and a maximum conversion of 96.2% was obtained for oleic acid conversion to biodiesel. All the studies show that MOF-supported solid acid catalysts also constitute efficient and stable heterogeneous catalysts for biodiesel production.

We wish to state that the use of porous and stable catalyst support is also crucial for catalyst performance and stability. Owing to the challenges of filtering the tiny catalyst particles and the high catalyst cost, heterogeneous acid catalysts such as sulfated titanium oxide have not been widely used in commercial biodiesel production operations. Zinc oxide and lead oxide are promising catalysts for both transesterification and esterification, but they are prone to leaching and have negative reuse effects.[35] This problem is also common with several homogeneous and heterogeneous acid catalysts.[36] Therefore, incorporation of proper support is also very important to improve the reusability of the catalyst and reduce leaching problems. Pure oxides are mostly supported by activated carbon, silica, and alumina.[35] In many cases, conventional support materials (such as activated carbon, alumina, and silica) are inefficient.[35] Therefore, zeolites, which have high porosity, large surface area, high acidity, and high hydrothermal stability than alumina and silica, may display improved metal−support interaction, resulting in improved catalyst stability.

$\beta$-zeolite is a form of zeolite that is rich in silica with a three-dimensional structure of intersecting 12-membered ring channel.[37] Several acid-catalyzed reactions can be carried out efficiently due to the relatively large channel structure.[37] Other factors influencing reaction efficiency of $\beta$-zeolite are the high thermal stability, large surface area, and tunable acidity in the protonic form.[38] It has been found that $\beta$-zeolite is an effective catalyst for transesterification, which could be utilized in the production of a vast array of products.[18,38] Transesterification occurs at the $\beta$-zeolite Brønsted acidic sites, which can be


https://doi.org/10.1021/acsomega.3c01892
ACS Omega 2023, 8, 23720−23732

Scheme 1. Schematic Showing Synthesis of H-β-Zeolite[a]

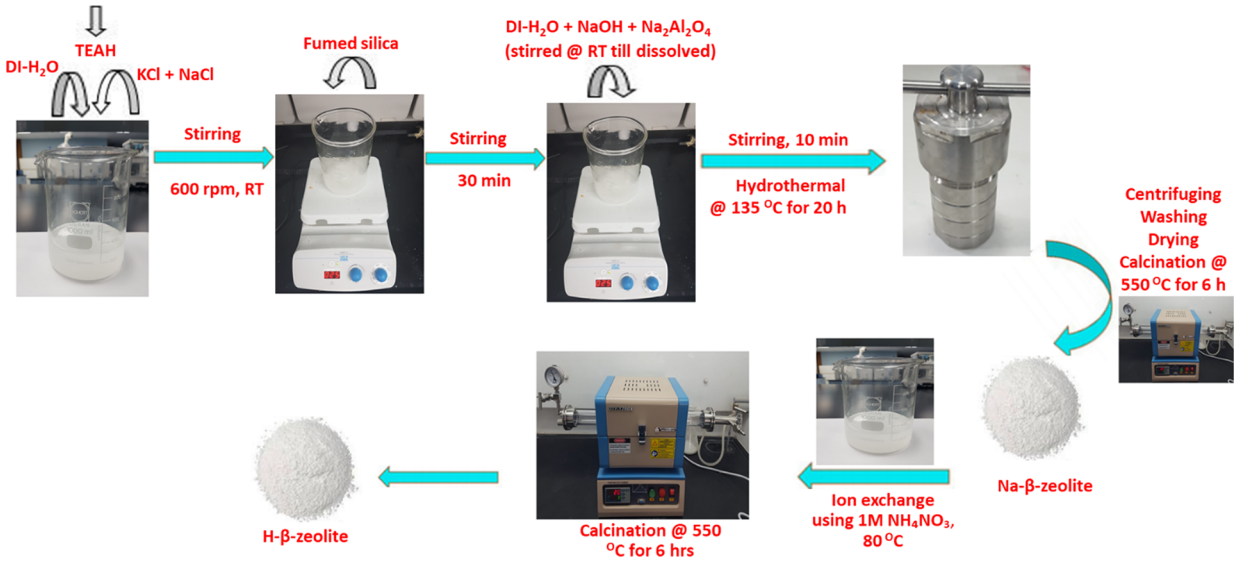


[a]Corresponding schematics for ZnO-β-zeolite and $SO_4^{2-}$/ZnO-β-zeolite are shown in Figure S1.

slightly altered with cation modifications, resulting in modified catalysts with appropriate acidity to fit diverse transesterifications.[38−40]

In the present study, we prepared β-zeolite, zinc oxide, and sulfated-zinc oxide supported on β-zeolite (ZnO-β-zeolite and $SO_4^{2-}$/ZnO-β-zeolite, respectively) and investigated their catalytic performance in the production of biodiesel using WCO. The parameters that affect reactions such as reaction time, the ratio of methanol to oil, catalyst loading, and temperature were optimized. A kinetic study was also conducted at different reaction temperatures to evaluate the rate of reaction and determine the activation energy ($E_a$). The surface acidity (Lewis or Brønsted) and its influence on the activity of pure β-zeolite, ZnO-β-zeolite and sulfated/ZnO-β-zeolite were also investigated. A sulfated/ZnO-β-zeolite catalyst was found to exhibit a significant amount of acidity relevant to high biodiesel conversion. The superiority of the $SO_4^{2-}$/ZnO-β-zeolite catalyst over ZnO-β-zeolite and pure β-zeolite was attributed to a number of physico-chemical characteristics such as pore size, acidity, and so forth, which resulted from the dispersion of the active phase caused by sulfate incorporation into the catalyst matrix.

## 2. EXPERIMENTAL SECTION

**2.1. Materials.** WCO was obtained from staff residence at King Fahd University of Petroleum and Minerals, Saudi Arabia. All chemicals were of analytical quality and utilized just as they were received, without additional purification. Methanol (purity >99%), zinc nitrate hydrate, tetraethylammonium hydroxide (40 wt % TEAH), sodium chloride (reagent grade), ammonium nitrate, sulfuric acid, and potassium chloride (reagent grade) were purchased from Sigma-Aldrich (USA). Also, fumed silica (amorphous silicon dioxide particles produced in an oxygen-hydrogen flame), sodium hydroxide (98%), and sodium aluminate (56 wt % $Al_2O_3$, 37 wt % $Na_2O$) were purchased from Sigma-Aldrich (USA).

**2.2. Synthesis of Catalysts.** *2.2.1. Synthesis of β-Zeolite.* The hydrothermal method described by Camblor et al. was used to produce β-zeolite,[40] using tetraethylammonium hydroxide as a structure-directing agent. In a typical procedure, 59.4 g of deionized water and 89.60 g of tetraethylammonium hydroxide (40%) were mixed with 0.53 g of sodium chloride and 1.44 g of potassium chloride and agitated until dissolved. Subsequently, fumed silica (30.0 g) was added to the mixture and agitated until homogenized. Then, sodium hydroxide (0.33 g) and sodium aluminate (1.79 g) were dissolved in deionized water (20.0 g) and stirred till completely dissolved. Following that, the two resulting liquids were mixed and stirred for 10 min. After stirring for 10 min, the thick gel formed was heated for 20 h at 135 °C in an autoclave. Following a hydrothermal reaction, the mixture was cooled in cold water and centrifuged. After centrifugation, the resulting mixture was dried at 77 °C after being washed with distilled water. The solid product that was produced after drying was calcined in a muffle furnace at 550 °C for 6 h. The sodium form of β-zeolite was thereby produced (Na-β-zeolite).

Using an ion-exchange method, Na-β-zeolite obtained was transformed into H-β-zeolite. Na-β-zeolite was impregnated with 1 M ammonium nitrate solution (1.0 g sample vs 20 mL 1 M $NH_4NO_3$) for 4 h at 80 °C. After two cycles of $Na^+/NH_4^+$ ion-exchanged β-zeolite, the resulting product was subjected to filtration, followed by washing with distilled water before drying at 100 °C overnight. The calcination of $NH_4$-β-zeolite for transformation to H-β-zeolite was carried out at 550 °C for 6 h in a muffle furnace. H-β-zeolite is the name given to the final sample obtained (Scheme 1).

*2.2.2. Synthesis of ZnO-β-Zeolite.* In a typical synthesis, zinc oxide supported on β-zeolite (ZnO-β-zeolite) was prepared by adding a predetermined amount of zinc nitrate hydrate (equivalent to 10 wt % of β-zeolite) and an appropriate amount of β-zeolite to 15 mL of distilled water and agitated at a temperature of 60 °C for 3 h at 600 rpm. After stirring for 3 h, the resulting precipitated solid was dried for 8 h at 100 °C. Finally, the solid obtained was calcined at 550 °C for 6 h, as shown in Scheme S1a.

*2.2.3. Synthesis of $SO_4^{2-}$/ZnO-β-Zeolite.* $SO_4^{2-}$/ZnO-β-zeolite was prepared by slowly adding a predefined amount of zinc nitrate hydrate and an appropriate amount of β-zeolite to 20 mL of 0.5 M sulfuric acid solutions and vigorously stirring at 60 °C for 3 h at a speed of 600 rpm. After stirring, the


https://doi.org/10.1021/acsomega.3c01892
ACS Omega 2023, 8, 23720−23732

resultant solid precipitate was filtered, oven-dried for 8 h at 100 °C, and calcined for 6 h at 550 °C in a muffle furnace [Scheme S1b].

**2.3. Catalyst Characterization.** The synthesized materials were thoroughly characterized in order to determine their structural, physical, and chemical characteristics. The crystalline structures of the catalytic materials were examined using various techniques. A Rigaku Ultima IV X-ray diffractometer was used to perform XRD on the catalysts, with a scan range of 5°−80° (2-theta) and a speed of 5.0°/min. The textural properties of the as-synthesized materials were measured utilizing Micrometrics ASAP 2020 equipment. (Micrometrics, USA). Pore size distribution of the catalytic materials was investigated utilizing the Barrett, Joyner, and Halenda technique. The surface area was determined using the Brunauer, Emmett, and Teller (BET) technique. Prior to the analysis, a vacuum pretreatment process at 250 °C with nitrogen gas flow was carried out for 3 h. Fourier transform infrared (FTIR) was utilized to determine the functional groups present in the catalysts. A Nicolet 6700 FT-IR spectrometer (Thermo Fisher Scientific, USA) was utilized to obtain FTIR spectra (wavenumber ranging from 400−4000 $cm^{-1}$). Pyridine-FTIR was used to measure the catalyst's acidity. In a typical procedure, the sample was put into a Specac cell and pretreated at 500 °C for 1 h under vacuum, and then the temperature was reduced to 150 °C. Pyridine vapor was flowed for 30 min. Following that, the samples were degassed under vacuum conditions at 150 °C in order to remove excess pyridine, and then at 150 °C, the acidity owing to Brønsted acid and Lewis acid site was measured. We examined the surface characteristics of the catalyst using a scanning electron microscope: Thermo Scientific Quattro ESEM equipped with an electron gun, a secondary electron mode, and a backscattered electron mode. An SDT Q600 thermogravimetric analyzer was used for the thermogravimetric analysis (TGA) (Thermal analysis instrument, USA), for which the samples were heated from 26 to 800 °C with an air flow rate of 10 °C/min.

**2.4. Biodiesel Synthesis.** Typically, a 50 mL autoclave made of stainless steel and fitted with a magnetic stirrer was used to perform the reaction. The reactor was filled with the required quantities of WCO, methanol, and catalysts. Afterward, the reaction system was agitated and heated until the desired temperature was reached. Following the mixture's cooling, the catalyst was centrifuged. The resulting sample mixture was allowed to settle (separated into two distinct layers: oil phase and aqueous phase). Fatty acid methyl esters (FAMEs) constituted the main component of the oil phase, while glycerol, methanol, and water were the components of the aqueous phase.

**2.5. Determination of Biodiesel Yield.** $^1$H NMR spectroscopy was utilized to determine the conversion of WCO to FAMEs. The biodiesel product was evaluated using a Bruker NMR 400 MHz spectrometer with deuterated chloroform ($CDCl_3$) as a solvent, in which case 10 mg of biodiesel product was dissolved in 1 mL of deuterated chloroform with 0.05% tetra-methyl silane.

The percent conversion of biodiesel to methyl ester was calculated according to eq 1:

$$C\ (\%) = [(2A_{ME})/(3A_{CH2})] \times 100 \quad (1)$$

where $A_{ME}$ represents the integrated peak area of the methoxy proton in the methyl ester, and $A_{CH2}$ represents the integrated peak area of the methylene proton adjacent to the carbonyl group. The percentage of oil converted to biodiesel is denoted by $C$.[41]

## 3. RESULTS AND DISCUSSION

**3.1. Characterization of the Catalyst.** *3.1.1. XRD Analysis.* One of the most common characterizations for heterogeneous catalysts is XRD analysis.[23,31−33] Figure 1 shows the XRD patterns of the three catalysts prepared in this work. Figure 1 shows the XRD patterns of the catalysts. It was observed that the synthesized H- $\beta$-zeolite has the XRD pattern exhibiting representative Bragg reflection conforming to the $\beta$-zeolite structure and a well-preserved crystalline structure, which is comparable to the findings that were previously reported in the literature.[42,43] The diffraction peak at $2\theta$ = 6°−8°, ascribed to (101) reflection of $\beta$-zeolite topology, is generally seen as an evidence of a highly distorted structure resulting from various isomorphs in the zeolite structure.[44] The narrow main distinct signal at $2\theta$ = 22°−23°, assigned to (302) reflection of $\beta$-zeolite, indicates zeolite structure lattice expansion/contraction.[45] Following the incorporation of Zn species and sulfonate group, the typical $\beta$-zeolite diffraction peak at 22°−23° slightly decreased in intensity, indicating a slight compression of the $\beta$-zeolite crystalline structure in the presence of zinc species without changing the framework of the zeolite and this is consistent with previous reports.[46,47] As illustrated in Figure 1, the zinc oxide is well incorporated into the $\beta$-zeolite support. The peaks at $2\theta$ = 31.7°, 34.4°, 36.2°, 56.5°, and 62.9° corresponding to (100), (002), (101), (110), and (103) lattice planes were attributed to the phase of zinc oxide, suggesting the formation of the crystals.[48] In addition, no diffraction peaks for $ZnSO_4$ were detected in $SO_4^{2-}$/ZnO-$\beta$-zeolite, which may be due to uniform distribution of sulfate species over the zeolite crystals' surface, in agreement with the literature.[49] These results, which are in agreement with previous literature reports on solid acid catalysts,[29−36] provide evidence of the crystallinity of the catalysts and the incorporation of zinc and sulfonate species into the $\beta$-zeolite structure.

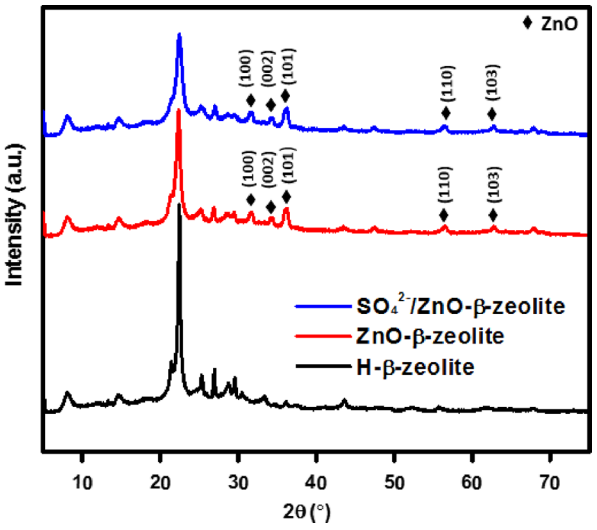


**Figure 1.** XRD patterns of the three catalysts. Peaks corresponding to lattice planes of ZnO are shown.



https://doi.org/10.1021/acsomega.3c01892
ACS Omega 2023, 8, 23720−23732

*3.1.2. FTIR Analysis.* FTIR is another important analytical technique used for the characterization of catalysts, given that it has the capability to delineate the different functional groups present in the catalyst system.[50−53] Thus, we have employed this technique to characterize the molecular composition of the catalysts. The FTIR spectra of synthesized catalysts are depicted in Figure 2. The band around 575 $cm^{-1}$ is

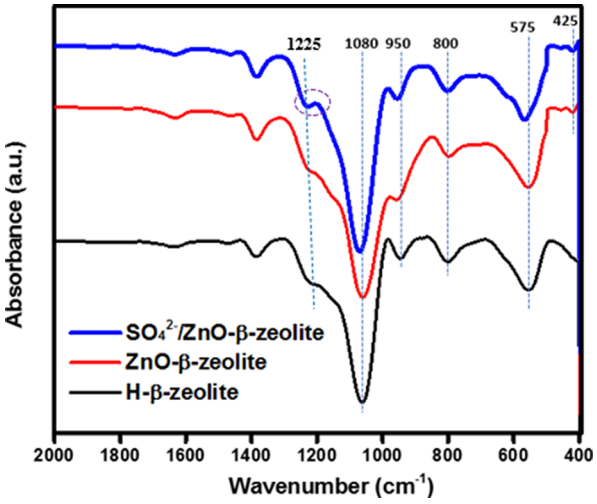


**Figure 2.** FTIR spectra of the three catalysts.

characteristic of *β*-zeolite since the structure contains six-membered rings.[50] The bands at about 800 and 1080 $cm^{-1}$ represent the T−O−T (T = Al or Si) symmetric stretching vibrations, which are susceptible to the aluminum composition of the framework.[51] The band that appears at 1225 $cm^{-1}$ is related to asymmetric stretching of the T−O−T.[51] Based on previous reports on different siliceous zeolites, the 950 $cm^{-1}$ band represents the stretching vibrations of Si−O and it belongs to uncoupled $SiO_4$ tetrahedron.[52,53] As seen in Figure 2, the structural vibration is comparable for all samples under investigation, confirming that the incorporation of metal oxide into *β*-zeolite support does not affect the structure. The band at 425 $cm^{-1}$ is related to the zinc oxide stretching mode, suggesting that ZnO is incorporated into the zeolite framework, which is consistent with the literature.[48] In addition, the intensity of the peak at 1225 $cm^{-1}$ is stronger (sharper) in $SO_4^{2-}$/ZnO-*β*-zeolite than in H-*β*-zeolite and ZnO-*β*-zeolite because of the incorporation of the sulfate species, which is related to S═O bonding in $SO_4^{2-}$.[49] Given the spectral signatures obtained from our FTIR measurements, we can say that the metal and sulfonate species are well incorporated into the *β*-zeolite support framework.

*3.1.3. Pyridine-FTIR Analysis.* Pyridine-FTIR involves the use of pyridine as a probe molecule, and it is a useful method for quantitative analysis of the Brønsted and Lewis acid sites present on a catalyst surface. It is widely applied in industrial and laboratory settings for quantifying acidic sites on the surface of a catalyst. Therefore, we performed pyridine-FTIR analysis on the catalysts in order to determine acidity, which is related to catalytic performance. Figure 3 shows the pyridine-adsorbed FTIR spectrum of the catalysts measured at 150 °C between 1430 and 1800 $cm^{-1}$. As seen in the figure, there are sharp adsorption bands resulting from the stretching of C−C bond of pyridine. Pyridine molecules interacting with Lewis (L) acid sites have sharp adsorption bands at 1456 and 1630

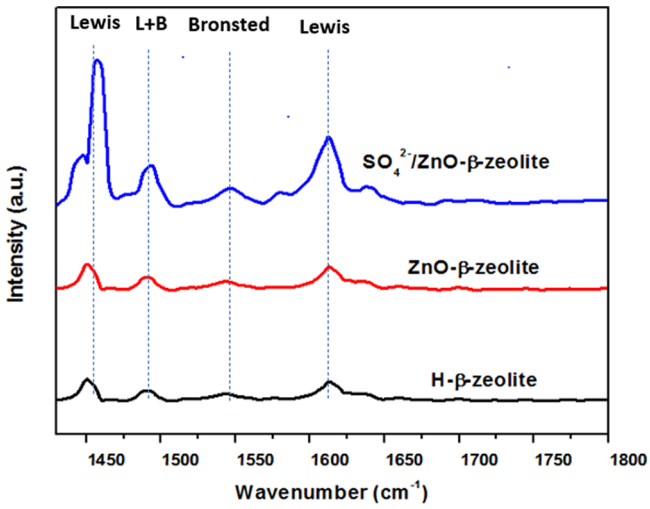


**Figure 3.** Pyridine-FTIR spectra of the catalysts.

$cm^{-1}$, while pyridine molecules adsorbed on Brønsted (B) acid sites have a band at 1550 $cm^{-1}$. A pyridine molecule interacting with both L and B acid sites was assigned to the band at 1490 $cm^{-1}$, in agreement with a previous study.[54] Also, we observe that the intensity of all the bands is substantially higher in $SO_4^{2-}$/ZnO-*β*-zeolite than in H-*β*-zeolite and ZnO-*β*-zeolite, indicating an increase in total acid sites. Conversely, the lower FTIR intensities in H-*β*-zeolite and ZnO-*β*-zeolite indicate very low acidity in both cases,[23] which is responsible for lower conversion of the WCO to biodiesel when these two catalysts were used (*vide infra*). The deposition of sulfated groups in the case of the $SO_4^{2-}$/ZnO-*β*-zeolite catalyst is responsible for the increase in total acid sites, which in turn is responsible for the more intense absorption bands shown for this catalyst (Figure 2). Thus, the result suggests that the prepared $SO_4^{2-}$/ZnO-*β*-zeolite has high acidity and can be utilized as a heterogeneous acid catalyst in biodiesel production.

*3.1.4. Textural Properties Analysis.* The $N_2$ adsorption−desorption isotherms of the catalysts are shown in Figure 4. A type-1 isotherm is observed in the H-*β*-zeolite.[55] The type-1 isotherm pattern suggests a micro-meso hierarchical porous textural characteristics.[55] The type-1 isotherm remains the same after zinc oxide loading on the *β*-zeolite support. The

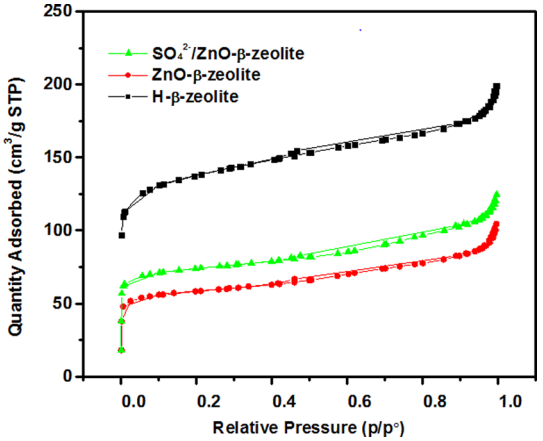


**Figure 4.** $N_2$ adsorption−desorption isotherms plot of H-*β*-zeolite support and the catalysts.



https://doi.org/10.1021/acsomega.3c01892
ACS Omega 2023, 8, 23720−23732

Table 1. Textural Properties of Supporting H-Beta Zeolite and the Catalysts

| sample | $S_{BET}$ ($m^2/g$) | $S_{micro}$ ($m^2/g$) | $S_{meso}$ ($m^2/g$) | $V_{micr}$ ($cm^3/g$) | $V_{total}$ ($cm^3/g$) | PS (nm) |
|---|---|---|---|---|---|---|
| H-$\beta$-zeolite | 469.21 | 317.72 | 151.48 | 0.14 | 0.28 | 4.52 |
| ZnO-$\beta$-zeolite | 198.01 | 140.72 | 57.27 | 0.06 | 0.13 | 6.46 |
| $SO_4^{2-}$/ZnO-$\beta$-zeolite | 250.26 | 180.27 | 69.99 | 0.08 | 0.17 | 6.50 |

pore size, volume, and specific surface areas of the catalysts are shown in Table 1. The surface area of $\beta$-zeolite was 469.21 $m^2/g$, while ZnO-$\beta$-zeolite and $SO_4^{2-}$/ZnO-$\beta$-zeolite had surface areas of 198.01 and 250.26 $m^2/g$, correspondingly. The reduction in the surface area could be attributed to pore blockage caused by metal oxide deposition on the $\beta$-zeolite. The catalyst is mostly found on the surface of zeolite support. As a result, the decrease in the support surface area is unimportant in this case because the primary role of zeolites is holding metal oxide particles together and preventing metal leaching.[56] Nevertheless, when the metal oxide is incorporated into the zeolite support, the pore size changes, and it increases upon incorporating both metal oxide and sulfate groups. The active phase dispersion caused by sulfate incorporation in the $SO_4^{2-}$/ZnO-$\beta$-zeolite catalyst matrix was also attributed to the high surface area and pore size of $SO_4^{2-}$/ZnO-$\beta$-zeolite compared to ZnO-$\beta$-zeolite. In a study involving PMA@Bi-BTC catalyst for biodiesel production from oleic acid,[32] the surface area and pore volume of the resulting catalyst increased on impregnation of PMA into Bi-BTC due to the interaction of the PMA with the Bi-BTC framework. Thus, in the present work, the incorporation of the metal oxide and sulfate species in the $\beta$-zeolite resulted in the observed increase in surface area and pore size. When producing biodiesel with a heterogeneous acid catalyst, this phenomenon is important. This could be because catalysts with larger pores reduce diffusion restrictions, particularly for long alkyl chain molecules.[47]

*3.1.5. Thermogravimetric Analysis.* The thermal stabilities of H-$\beta$-zeolite, ZnO-$\beta$-zeolite, and $SO_4^{2-}$/ZnO-$\beta$-zeolite were established with TGA. In general, the TGA curve depicts the stages of weight loss in the samples (Figure 5). According to

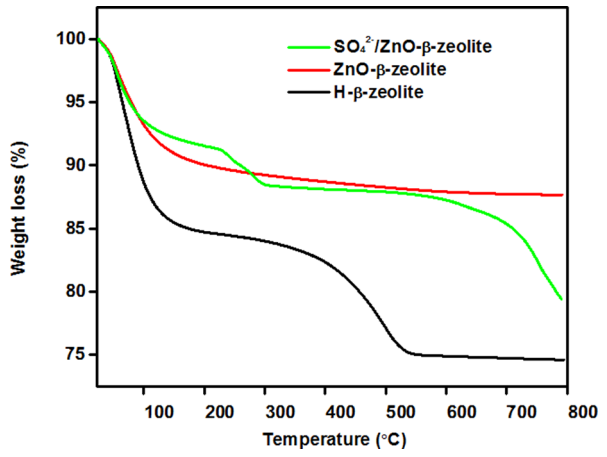


Figure 5. TGA analysis of the catalysts.

the literature, weight loss below 350 °C can be ascribed to the removal of physically adsorbed water and the thermal degradation of noninteracting tetraethylammonium hydroxide (TEAOH) species, whereas weight loss above 350 °C can be attributed to the pyrolysis of tetraethylammonium cation ($TEA^+$) interacting with the framework of zeolite.[40] This effect leads to a weight loss of about 10−15%. The extra weight loss in this temperature range could be related to lower temperature decomposition residues. As seen in Figure 5, the weight loss of about 5−15% observed in the three catalysts in the 100−200 °C temperature range is ascribed to physically adsorbed water, while the weight loss of about 5% observed between 200 and 300 °C may be due to loss of water trapped within the composite framework and thermal degradation of TEAOH.[32,33] Further weight loss observed for H-$\beta$-zeolite in the 400−500 °C temperature range may be due to the pyrolysis of $TEA^+$.[40] After the weight loss around 100−300 °C, the catalysts are essentially stable. Accordingly, we can argue that the catalysts show high thermal stability, as the main decomposition of the zeolite support started at high temperature, which indicates the high stability of $\beta$-zeolite. Thus, the results showed that the synthesized catalysts are thermally stable and can be utilized to produce biodiesel.

*3.1.6. SEM Analysis.* Figure 6 shows the SEM images depicting the morphology of the catalysts. The morphology of the prepared H-$\beta$-zeolite revealed uniform and spherical particles with sizes varying between 0.5−2 $\mu$m (Figure 6a), which is congruent with published research findings.[56] After zinc oxide had been loaded onto H-$\beta$-zeolite (ZnO-$\beta$-zeolite) and incorporation of both zinc oxide and sulfate groups in H-$\beta$-zeolite ($SO_4^{2-}$/ZnO-$\beta$-zeolite), there is no substantial change in the shape of the particles (Figure 6b,c). These results suggest that zinc oxide particles were uniformly dispersed on the surface of the $\beta$-zeolite, such that the three catalysts have similar morphology and appearance. The similar morphology displayed by all three catalysts reported in this work may not be out of place. Recently, Mao et al. also reported SEM images of their sulfamic acid (SA)-modified ZIF-90 catalysts that are every similar to each other despite different SA/ZIF-90 weight ratios being used.[31]

**3.2. Catalytic Performance of the Catalysts.** The performance of the synthesized catalysts was investigated for the methanolysis of WCO for biodiesel production. The catalytic activities of H-$\beta$-zeolite, ZnO-$\beta$-zeolite, and $SO_4^{2-}$/ZnO-$\beta$-zeolite were investigated at fixed process parameters such as reaction temperature of 200 °C, WCO/methanol molar ratio of 1:12, and catalyst loading of 2.0 wt % for 4 h. Figure 7 shows the biodiesel conversion trend when the catalysts were used. The highest WCO conversion was achieved by using ZnO-$\beta$-zeolite and $SO_4^{2-}$/ZnO-$\beta$-zeolite. This increase in catalytic activity is most likely due to the appropriate particle size. It should be emphasized that triglyceride access to $\beta$-zeolite internal sites may be limited due to their sizes; consequently, catalytic activity originates primarily from sites on the $\beta$-zeolite external surfaces. Due to the large size of zinc species, Zn ion exchange is expected to occur on the $\beta$-zeolite external surface, which can significantly increase the number of sites on the $\beta$-zeolite exterior surfaces. Thus, it can be inferred that the ZnO-$\beta$-zeolite and $SO_4^{2-}$/ZnO-$\beta$-zeolite has a greater number of external active sites available for the reactant. As depicted in Figure 7, ZnO-$\beta$-zeolite and $SO_4^{2-}$/ZnO-$\beta$-zeolite catalysts were more appro-


https://doi.org/10.1021/acsomega.3c01892
ACS Omega 2023, 8, 23720−23732

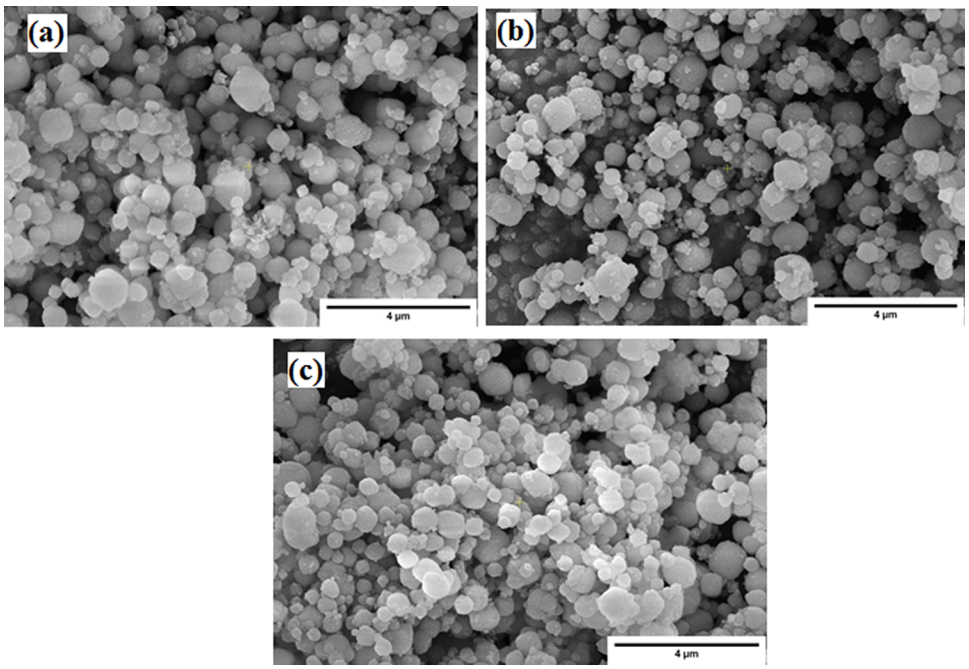


**Figure 6.** SEM images of the catalysts: (a) H-$\beta$-zeolite; (b) ZnO-$\beta$-zeolite; and (c) $SO_4^{2-}$/ZnO-$\beta$-zeolite.

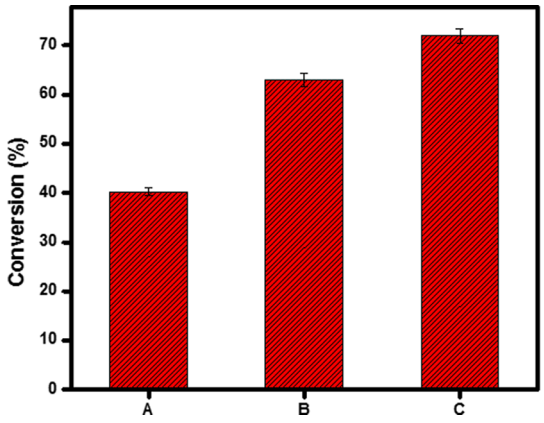


**Figure 7.** Catalytic performance of H-$\beta$-zeolite, ZnO-$\beta$-zeolite, and $SO_4^{2-}$/ZnO-$\beta$-zeolite catalysts related to conversion of WCO [A = H-$\beta$-zeolite, B = ZnO-$\beta$-zeolite, and C = $SO_4^{2-}$/ZnO-$\beta$-zeolite].

priate in terms of external accessibility to promote WCO conversion, which appears to be guided primarily by the improvement of characteristics of the $\beta$-zeolite external surface. Therefore, ZnO-$\beta$-zeolite and $SO_4^{2-}$/ZnO-$\beta$-zeolite catalysts were further compared for biodiesel production, and the process parameters (such as methanol to WCO molar ratio, catalyst loading, time, and temperature) were optimized.

**3.3. Biodiesel Analysis.** Following biodiesel synthesis as described in the experimental section, the conversion of WCO to FAME and biodiesel characterization were carried out using $^1$H NMR and $^{13}$C NMR spectroscopy, respectively. The $^1$H NMR spectrum of the biodiesel sample obtained after WCO conversion to FAME using the $SO_4^{2-}$/ZnO-$\beta$-zeolite catalyst is shown in Figure S1. The presence of a triplet peak at 2.31 ppm and a single peak at 3.67 ppm corresponding to $\alpha$-$CH_2$ protons ($A_{CH2}$) and methoxy protons ($A_{ME}$), respectively, confirms biodiesel formation.[28] These two peaks indicated oil conversion to biodiesel. Other peaks include signals at 0.88, 1.26, and 1.61 ppm for end-of-chain methyl protons, carbon methylene proton, and carbonyl methylene protons, respectively. The 5.35 ppm signal is attributed to an olefinic proton.[41,57,58] Eq 1 describes the oil conversion into biodiesel.[41] Using eq 1, the percentage conversion of WCO to equivalent FAMEs was found to be 96.9%.

Figure S2 depicts the $^{13}$C NMR spectra of WCO biodiesel. The ester carbonyl carbon (−COO−) peak was observed at 174.31 ppm, and the C−O carbon appears at 51.42 ppm in the biodiesel spectrum. The two signals at 127.90 and 130.19 ppm indicate the presence of unsaturated fatty acids. The 14.11 ppm signal corresponds to the end-chain methyl carbon, while the signals in the range of 22.69−34.10 ppm are related to aliphatic methylene groups (−$CH_{2\text{-}S}$) of FAMEs.[57,58] The composition of the WCO biodiesel was investigated using GC−MS analysis. The GC−MS chromatogram of the biodiesel sample is shown in Figure S3. Table S1 lists the components of the biodiesel. The biodiesel sample comprised both saturated and unsaturated FAMEs.

The performance property of the biodiesel product is compared with ASTM standards. The fuel properties such as flash point, kinematic viscosity, density, specific gravity, and acid value of the WCO-based biodiesel are shown in Table 2. The data conform to the recommended values specified in ASTM D6751. Therefore, the biodiesel product obtained in

**Table 2. Performance Properties of the WCO Biodiesel in Comparison with ASTM Standards**

| fuel properties | ASTM method used | ASTM D6751 biodiesel | WCO biodiesel |
|---|---|---|---|
| kinematic viscosity (40 °C, mm$^2$/s) | D445 | 1.9−6.0 | 5.04 |
| density (40 °C, g/cm$^3$) | D5002 | 0.86−0.90 | 0.871 |
| specific gravity (40 °C, g/cm$^3$) | D287 | 0.88 | 0.876 |
| flash point (°C) | D93 | 100−170 | 132 |
| acid value (mg KOH/g) | D664 | 0.5 | 0.15 |



https://doi.org/10.1021/acsomega.3c01892
ACS Omega 2023, 8, 23720−23732

the present study can be utilized either as a pure fuel or blended with conventional diesel fuel.

**3.4. Effect of Different Reaction Parameters.** To investigate the activity of the catalyst in biodiesel's production, WCO was reacted with methanol over ZnO-$\beta$-zeolite and $SO_4^{2-}$/ZnO-$\beta$-zeolite catalysts. Thus, different parameters affecting methyl ester conversion were examined here. The effects of experimental parameters such as the molar ratio of methanol to oil (MRMO), catalyst loading, time, and temperature were investigated. Figures 8 and 9 depict the results of the parametric investigation for biodiesel production, while varying the experimental conditions.

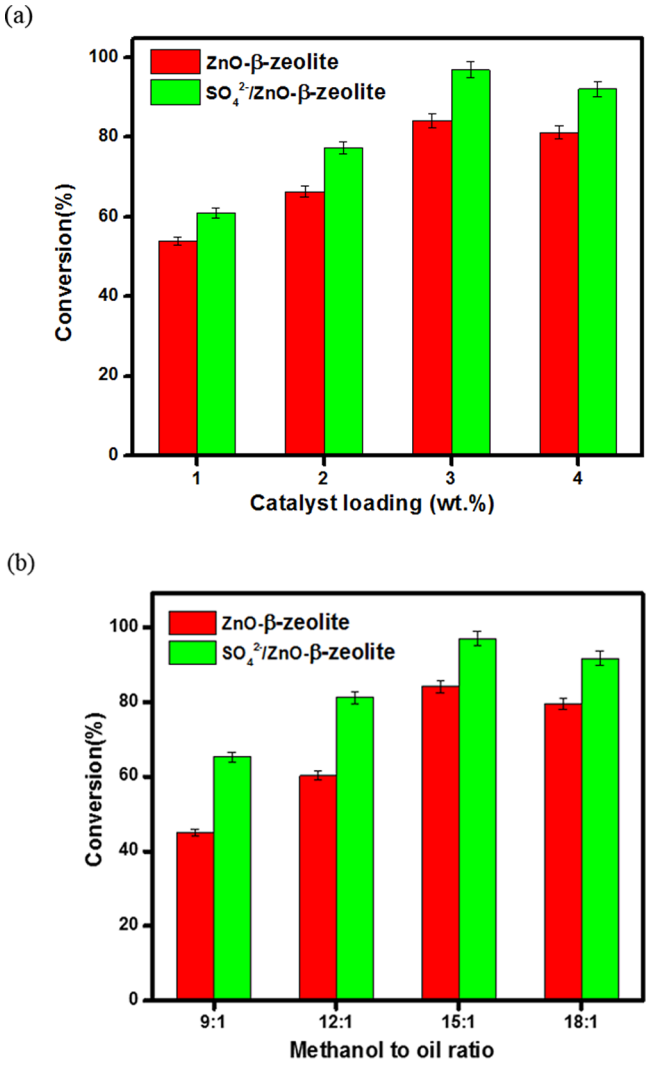


**Figure 8.** Effects of (a) catalyst loading and (b) molar ratio of methanol to oil.

*3.4.1. Effect of Catalyst Loading and Methanol/Oil Ratio.* In order to investigate the impact of catalyst loading on biodiesel conversion, the amount of catalyst used was varied from 1.0 to 4.0 wt % (Figure 8a). At a constant MRMO of 15:1, 8 h reaction time, and 200 °C, increase in catalyst loading from 1.0 to 3.0 wt % steadily enhanced biodiesel conversion, reaching a maximum of 84.1% for ZnO-$\beta$-zeolite and 96.9% for $SO_4^{2-}$/ZnO-$\beta$-zeolite. Increased catalyst loading above 3.0 wt % reduces biodiesel conversion due to a mixing problem that involves solid catalyst, reactant, and product.[39,59] Moreover, if

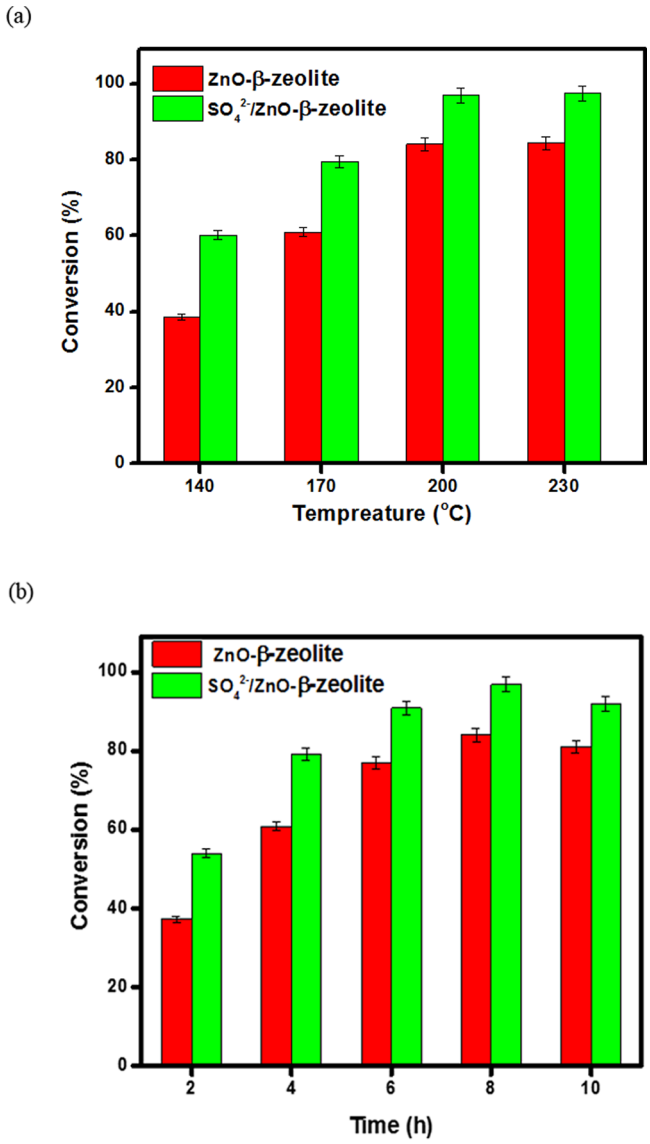


**Figure 9.** Effects of (a) reaction temperature and (b) reaction time.

catalyst loading exceeds the optimum amount, biodiesel products can adsorb on the catalyst surface, reducing conversion.[41,60] Thus, the optimum catalyst loading for WCO conversion to biodiesel in this study is 3.0 wt %, and other reaction parameters were optimized at this loading.

Another factor that affects biodiesel conversion is the MRMO. Transesterification reaction requires one mole of oil and three moles of methanol to produce one mole of glycerol and three moles of FAMEs. Since the reaction is reversible, it is preferable to use excess methanol to favor the forward reaction. We varied the MRMO from 9:1 to 18:1 at 8 h reaction time, 200 °C and 3.0 wt % catalyst loading. We found that increasing the MRMO increases biodiesel conversion. When the MRMO rose to 15:1, the biodiesel conversion increased to 84.1 and 96.8% for ZnO-$\beta$-zeolite and $SO_4^{2-}$/ZnO-$\beta$-zeolite catalyst, respectively. However, beyond 15:1 MRMO, biodiesel conversion decreases. Increasing the MRMO might lead to incomplete transesterification and mass transfer limitation caused by dilution.[61] Therefore, optimum MRMO was kept at 15:1 in this study.



https://doi.org/10.1021/acsomega.3c01892
ACS Omega 2023, 8, 23720−23732

*3.4.2. Effect of Reaction Temperature and Time.* Temperature has a significant impact on reaction rate, and so one of the most important parameters to optimize is the reaction temperature. Also, the formation of three immiscible phases consisting of oil, methanol, and solid acid catalyst at the beginning of the reaction limits mass transfer; therefore, high temperature is required when a heterogenous acid catalyst is employed. Most studies reported that high temperature favor biodiesel conversion from low-grade material/WCO feedstock.[19,21] Figure 9a depicts biodiesel conversion as reaction temperature changes. The reaction temperature was varied from 140 to 230 °C, at 8 h reaction time, MRMO of 15:1 and 3 wt % catalyst loading. At lower reaction temperatures, the biodiesel conversion was very low (Figure 9a). However, the reactants acquired sufficient kinetic energy at higher temperatures to enhance the system's mass transfer rate, resulting in the optimum conversion of 84.1 and 96.9% for ZnO-$\beta$-zeolite and $SO_4^{2-}$/ZnO-$\beta$-zeolite catalyst, respectively, at 200 °C. When the temperature rose beyond 200 °C, the biodiesel conversion remained unchanged. Hence, 200 °C is considered the optimal reaction temperature in this study.

The impact of reaction time on biodiesel conversion was also investigated by varying the reaction time from 2 to 10 h at 2-hour intervals with a catalyst loading of 3.0 wt % and a 15:1 MRMO (Figure 9b). The result showed that the heterogeneous catalyst had not yet been fully activated in the first 2 h of reaction, resulting in a slow reaction rate and low biodiesel conversion. However, increasing the reaction time to 8 h increases biodiesel conversion to maximum values of 84.2 and 96.9% for the ZnO-$\beta$-zeolite and $SO_4^{2-}$/ZnO-$\beta$-zeolite catalysts, respectively. After 8 h, there was a decrease in biodiesel conversion. This behavior could be attributed to reverse transesterification between FAMEs and glycerol as reaction time increases.[62,63] The optimal reaction time for biodiesel production was thus taken to be 8 h. We note that the activity of the $SO_4^{2-}$/ZnO-$\beta$-zeolite catalyst was higher than that of the ZnO-$\beta$-zeolite catalyst, and this behavior may be attributed to the highly acidic nature of the $SO_4^{2-}$/ZnO-$\beta$-zeolite catalyst.

**3.5. Kinetic Studies of Biodiesel Synthesis.** The kinetics of WCO biodiesel production was studied utilizing the $SO_4^{2-}$/ZnO-$\beta$-zeolite catalyst at varying temperatures (140 to 230 °C) under optimum reaction conditions, and the reaction activation energy ($E_a$) was thereby computed. The reverse reaction can be ignored since an excess amount of methanol was employed, and the pseudo-first-order model is assumed to govern the reaction.[64,65] Therefore, eq 2 fits the reaction rate constant,[66] while the activation energy ($E_a$) of the process is computed using the Arrhenius eq 3.[66]

$$k = -\ln \frac{1 - X}{t} \tag{2}$$

$$\ln k = \ln A - \frac{E_a}{RT} \tag{3}$$

where $R$ = universal gas constant (8.314 J mol$^{-1}$ K$^{-1}$); $A$ = Arrhenius constant; $T$ = reaction temperature (Kelvin); $X$ = conversion of WCO at time $t$; $k$ = reaction rate constant.

According to eq 2, a plot of $-\ln(1 - X)$ versus time is linear, as depicted in Figure 10a. The plots show that the model is acceptable for pseudo-first order kinetics due to its good linearity and high regression coefficients. A linear plot of $\ln k$ against $1/T$ that shows a high regression coefficient is depicted in Figure 10b. According to the Arrhenius plot, the activation energy ($E_a$) of the reaction was 38.58 kJ/mol using the $SO_4^{2-}$/ZnO-$\beta$-zeolite catalyst. The activation energy obtained from the WCO is consistent with the literature and is comparable to the activation energy achieved for soybean oil transesterification (i.e., 33.6−84 kJ/mol).[67,68] Moreover, a value of $E_a$ greater than 15 kJ/mol indicates that the reaction is controlled chemically.[54]

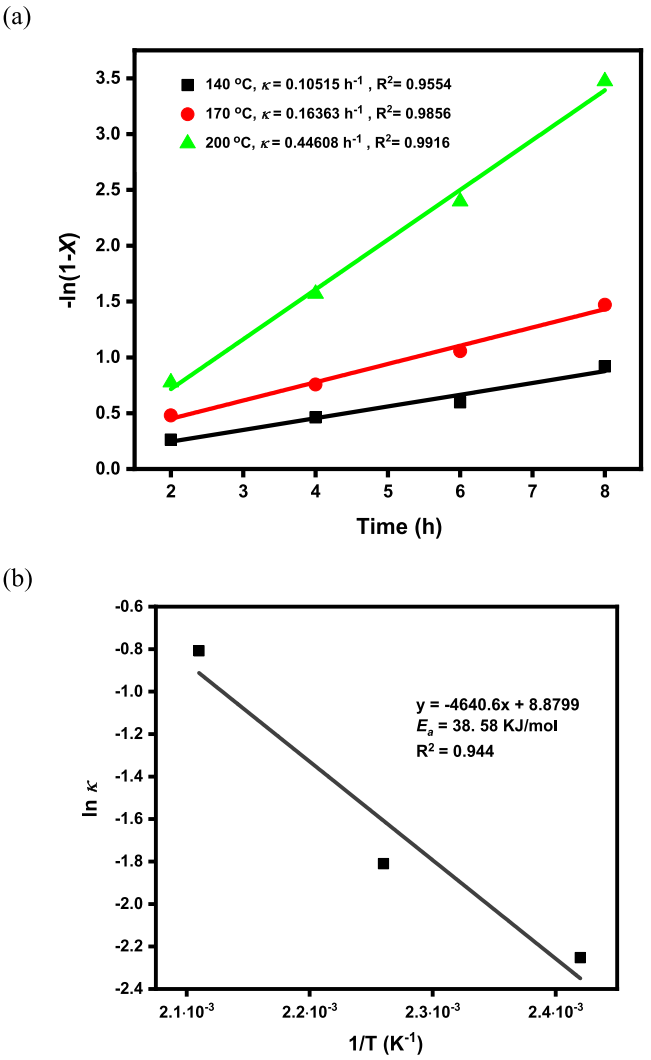


**Figure 10.** (a) Graph depicting the relationship between $-\ln(1 - X)$ and time; and (b) Arrhenius graph showing the relationship between $k$ and $1/T$.

**3.6. Plausible Mechanism.** Figure 11 shows a plausible mechanism for simultaneous transesterification and esterification of WCO. The carbonyl group of fatty acid/triglyceride is typically adsorbed on the $SO_4^{2-}$/ZnO-$\beta$-zeolite catalyst to produce the protonated carbonyl group, which is then attacked by the nucleophilic oxygen atom from methanol's hydroxyl group to form a tetrahedral intermediate. Finally, in the esterification reaction, the tetrahedral intermediate removes water to produce methyl ester. This intermediate removes glycerol during the transesterification reaction to produce a new methyl ester.

**3.7. Reusability of Catalysts.** Solid catalysts have the primary advantage of being reusable. The reusability of the catalyst was examined in this work (Figure 12). To evaluate


https://doi.org/10.1021/acsomega.3c01892
ACS Omega 2023, 8, 23720−23732

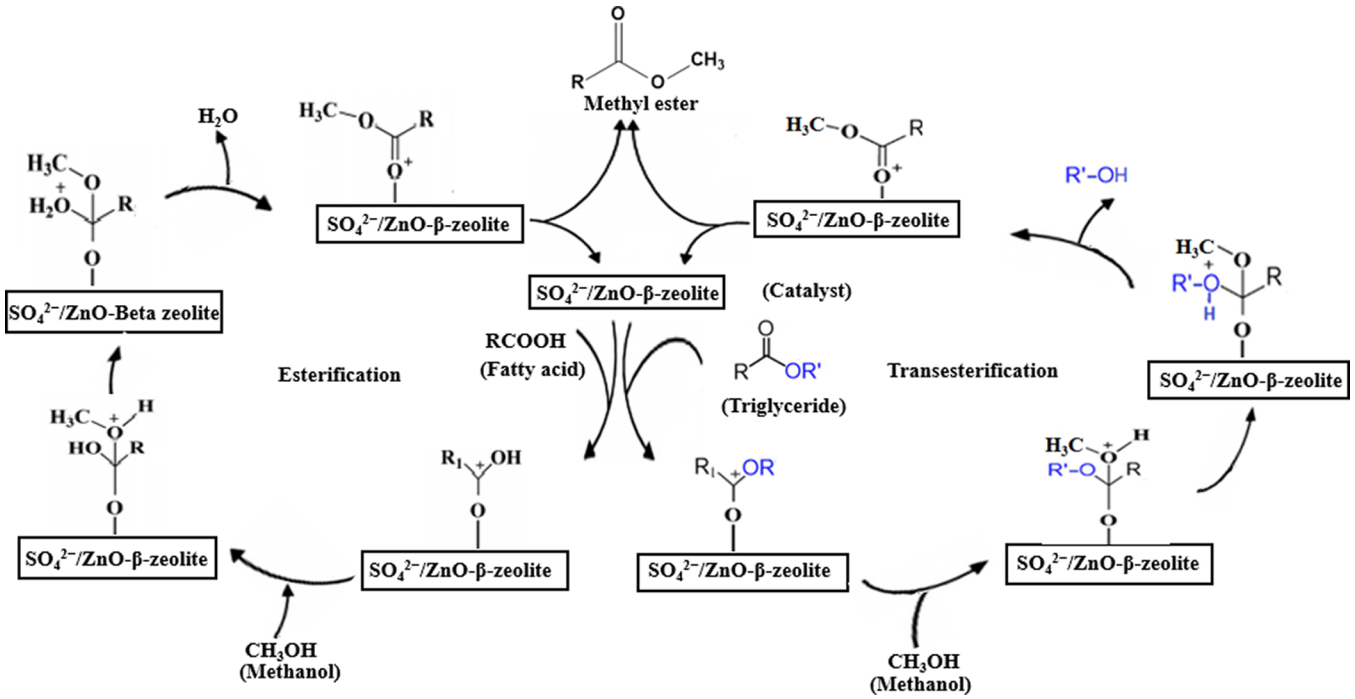


**Figure 11.** Plausible mechanism for concurrent esterification and transesterification reactions.

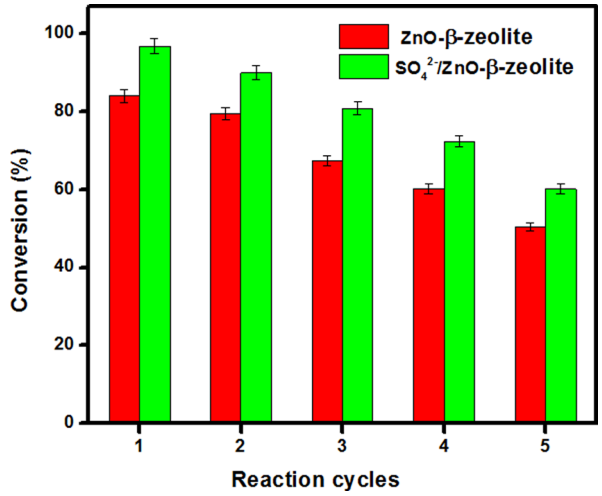


**Figure 12.** Reusability potential of the ZnO-treated catalysts.

catalyst reusability, both ZnO-*β*-zeolite and $SO_4^{2-}$/ZnO-*β*-zeolite catalysts were centrifuged from the reaction mixture, rinsed with methanol, oven-dried at 100 °C for 12 h, and then used immediately after each run. Both transesterification and esterification reaction of WCO were carried out five times under the optimal conditions of 3.0 wt % catalyst loading at 200 °C and 15:1 MRMO for 8 h, and the results are shown in Figure 12. We found that the catalysts maintained fairly good stability even after three experiments retaining 67.49 and 80.89% for ZnO-*β*-zeolite and $SO_4^{2-}$/ZnO-*β*-zeolite catalyst, respectively, of its original activity. Furthermore, XRD analysis was conducted to determine the stability of the catalyst (see Figure S4). According to Figure S4, the XRD spectra of the five-recovery catalyst were nearly identical to that of the fresh one, except for a slight decrease in peak intensity, indicating the better recyclability of the two catalysts. The partial loss in activity was most likely due to the leaching part of the active component into the reaction media during repeated reactions. Therefore, these findings clearly show that the catalysts are highly recyclable.

Table 3 compares the performance of different heterogeneous catalysts in simultaneous transesterification and

**Table 3. Different Solid Catalysts' Performance in Biodiesel Production Utilizing Low Grade Material/Waste Oils as Feedstock**

| catalyst | operating conditions[a] | performance | reference |
|---|---|---|---|
| Mg−Al−CO3 hydrotalcite | 3 h, 200 °C, 1 wt %, 6:1 | 99% oil conversion | 68 |
| $SO_4^{-2}/TiO_2-SiO_2$ | 6 h, 200 °C, 3 wt %, 16:1 | 92% FAME yield | 19 |
| Zn3La1 | 3 h, 200 °C, 2.3 wt %, 36:1 | 96% FAME yield | 69 |
| zinc stearate immobilized on silica gel | 10 h, 200 °C, 3 wt %, 18:1 | 98% FAME yield | 70 |
| 12-tungstophosphoric acid supported on zirconia | 10 h, 200 °C, 3 wt %, 9:1 | 90% FAME yield | 71 |
| H-ZSM-5 | 4 h, 100 °C, 10 wt %, 45:1 | 55% oil conversion | 72 |
| H-ZSM-5 (1.0 M citric acid modified) | 4 h, 100 °C, 10 wt %, 45:1 | 84% oil conversion | 73 |
| $La_2O_3$/Na-Y-800 | 1 h, 70 °C, 10 wt %, 15:1 | 80% FAME yield | 61 |
| S-$La_2O_3$/Na-Y-800 (S = surfactant modified) | 1 h, 70 °C, 10 wt %, 15:1 | 84% FAME yield | 74 |
| CaO/zeolite | 1.25 h, 8 wt %, 30:1 | 90.85% FAME yield | 75 |
| ZnO-*β*-zeolite | 8 h, 200 °C, 3.0 wt %, 15:1 | 84.1% conversion | this work |
| $SO_4^{2-}$/ZnO-*β*-zeolite | 8 h, 200 °C, 3.0 wt %, 15:1 | 96.9% conversion | this work |

[a]The operating conditions (reaction time, temperature, catalyst loading, and MRMO).



https://doi.org/10.1021/acsomega.3c01892
ACS Omega 2023, 8, 23720−23732

esterification reactions using low-grade/waste oils as feedstock. Our catalysts' performance is comparable to other studies.

## 4. CONCLUSIONS

ZnO-$\beta$-zeolite and $SO_4^{2-}$/ZnO-$\beta$-zeolite catalysts, prepared by the wet impregnation approach, proved to be effective catalysts for simultaneous transesterification and esterification of WCO. The $SO_4^{2-}$/ZnO-$\beta$-zeolite catalyst exhibited remarkable catalytic activity in contrast to ZnO-$\beta$-zeolite. Characterization analyses show that when the sulfonate group is incorporated to the surface of the catalyst, Lewis/Brønsted acid sites are formed. These acid sites contribute to the large surface area, high acidity, and high dispersion of the active phase of the $SO_4^{2-}$/ZnO-$\beta$-zeolite. The highest WCO conversion of 96.9% was obtained using the $SO_4^{2-}$/ZnO-$\beta$-zeolite catalyst under the optimum reaction condition of 3.0 wt % catalyst loading, 200 °C reaction temperature, and 15:1 MRMO for 8 h. Kinetic studies show that simultaneous transesterification and esterification exhibit a pseudo-first order kinetic model, with an apparent activation energy of 38.58 kJ/mol. This result suggests that the reaction is chemically controlled and not by mass transfer and diffusion constraints. Furthermore, the $SO_4^{2-}$/ZnO-$\beta$-zeolite showed good stability, and after three cycles of use, biodiesel conversion was about 84% (indicating no significant loss of activity). The characteristics of WCO-derived biodiesel satisfy the requirements of the ASTM6751 standard. When compared with the performance of some heterogeneous acid catalysts used for biodiesel synthesis, the $SO_4^{2-}$/ZnO-$\beta$-zeolite reported in this work exhibits promising activity for biodiesel production from WCO. Regardless, given the catalysts operate at an optimal temperature of 200 °C, the activity and stability of the catalysts may be further improved by using the equilibrium adsorption method of catalyst preparation. This may reduce pore blockage of the $\beta$-zeolite support, improve WCO conversion, and enhance the stability of the catalyst. A future study should investigate this method of catalyst preparation for WCO conversion to biodiesel and compare the performance and stability of the resulting catalysts with the present work. Overall, the catalyst system reported in the present work has the potential to be used in industrial biodiesel production since it is capable of converting waste oil, low-grade oil, and inexpensive oil with a high FFA content into biodiesel.

## ■ ASSOCIATED CONTENT

### Supporting Information

The Supporting Information is available free of charge at https://pubs.acs.org/doi/10.1021/acsomega.3c01892.

Schematic of ZnO-$\beta$-zeolite and SO42−/ZnO-$\beta$-zeolite synthesis, $^1$H NMR spectrum of biodiesel obtained with $SO_4^{2-}$/ZnO-$\beta$-zeolite catalyst, $^{13}$C NMR spectrum of biodiesel obtained with the $SO_4^{2-}$/ZnO-$\beta$-zeolite catalyst, GC/MS chromatogram of FAMEs obtained with $SO_4^{2-}$/ZnO-$\beta$-zeolite catalyst, constituent FAMEs of biodiesel obtained with the $SO_4^{2-}$/ZnO-$\beta$-zeolite catalyst, XRD patterns of fresh and used $SO_4^{2-}$/ZnO-$\beta$-zeolite catalyst (PDF)

## ■ AUTHOR INFORMATION


### Corresponding Author

**Sulayman A. Oladepo** − *Department of Chemistry and Interdisciplinary Research Center for Advanced Materials (IRC-AM), King Fahd University of Petroleum and Minerals, Dhahran 31261, Kingdom of Saudi Arabia;* orcid.org/0000-0002-2041-0731; Phone: +966 13 860 7103; Email: saoladepo@kfupm.edu.sa; Fax: +966 13 860 4277

### Authors

**Basiru O. Yusuf** − *Department of Chemistry, King Fahd University of Petroleum and Minerals, Dhahran 31261, Kingdom of Saudi Arabia*

**Saheed A. Ganiyu** − *Department of Chemistry and Interdisciplinary Research Center for Refining and Advanced Chemicals (IRC-RAC), King Fahd University of Petroleum and Minerals, Dhahran 31261, Kingdom of Saudi Arabia*

Complete contact information is available at: https://pubs.acs.org/10.1021/acsomega.3c01892


### Notes

The authors declare no competing financial interest.

## ■ ACKNOWLEDGMENTS

The authors gratefully acknowledge Dr. Khalid Alhooshani, the Chemistry Department, and Deanship of Research Oversight and Coordination at King Fahd University of Petroleum and Minerals for making available funding and other resources used for this work.

## ■ REFERENCES


(1) Muradov, N. Low to Near-Zero CO2 Production of Hydrogen from Fossil Fuels: Status and Perspectives. *Int. J. Hydrogen Energy* **2017**, *42*, 14058−14088.

(2) Martins, F.; Felgueiras, C.; Smitková, M. Fossil Fuel Energy Consumption in European Countries. *Energy Procedia* **2018**, *153*, 107−111.

(3) Perera, F.; Ashrafi, A.; Kinney, P.; Mills, D. Towards a Fuller Assessment of Benefits to Children's Health of Reducing Air Pollution and Mitigating Climate Change Due to Fossil Fuel Combustion. *Environ. Res.* **2019**, *172*, 55−72.

(4) Bridges, A.; Felder, F. A.; McKelvey, K.; Niyogi, I. Uncertainty in Energy Planning: Estimating the Health Impacts of Air Pollution from Fossil Fuel Electricity Generation. *Energy Res. Soc. Sci.* **2015**, *6*, 74−77.

(5) Cui, D.; Deng, Z.; Liu, Z. China's Non-Fossil Fuel CO2 Emissions from Industrial Processes. *Appl. Energy* **2019**, *254*, No. 113537.

(6) Abreu, F. R.; Alves, M. B.; Macêdo, C. C. S.; Zara, L. F.; Suarez, P. A. Z. New Multi-Phase Catalytic Systems Based on Tin Compounds Active for Vegetable Oil Transesterificaton Reaction. *J. Mol. Catal. A: Chem.* **2005**, *227*, 263−267.

(7) Ambat, I.; Srivastava, V.; Sillanpä, M. Recent Advancement in Biodiesel Production Methodologies Using Various Feedstock: A Review. *Renewable Sustainable Energy Rev.* **2018**, *90*, 356−369.

(8) You, Y. D.; Shie, J. L.; Chang, C. Y.; Huang, S. H.; Pai, C. Y.; Yu, Y. H.; Chang, C. H. Economic Cost Analysis of Biodiesel Production: Case in Soybean Oil. *Energy Fuels* **2008**, *22*, 182−189.

(9) Kulkarni, M. G.; Dalai, A. K. Waste Cooking Oil - An Economical Source for Biodiesel: A Review. *Ind. Eng. Chem. Res.* **2006**, *45*, 2901−2913.

(10) Zhang, Y.; Dubé, M. A.; McLean, D. D.; Kates, M. Biodiesel Production from Waste Cooking Oil: 2. Economic Assessment and Sensitivity Analysis. *Bioresour. Technol.* **2003**, *90*, 229−240.

(11) Hussain, M. N.; Samad, T.; Al Janajreh, I. Economic Feasibility of Biodiesel Production from Waste Cooking Oil in the UAE. *Sustain. Cities Soc.* **2016**, *26*, 217−226.

(12) Canakci, M.; Van Gerpen, J. Biodiesel Production from Oils and Fats with High Free Fatty Acids. *Trans. Am. Soc. Agric. Eng.* **2001**, *44*, 1429−1436.

(13) Zullaikah, S.; Lai, C. C.; Vali, S. R.; Ju, Y. H. A Two-Step Acid-Catalyzed Process for the Production of Biodiesel from Rice Bran Oil. *Bioresour. Technol.* **2005**, *96*, 1889−1896.
(14) Wang, Y.; Ou, S.; Liu, P.; Xue, F.; Tang, S. Comparison of Two Different Processes to Synthesize Biodiesel by Waste Cooking Oil. *J. Mol. Catal. A: Chem.* **2006**, *252*, 107−112.
(15) Di Serio, M.; Ledda, M.; Cozzolino, M.; Minutillo, G.; Tesser, R.; Santacesaria, E. Transesterification of Soybean Oil to Biodiesel by Using Heterogeneous Basic Catalysts. *Ind. Eng. Chem. Res.* **2006**, *45*, 3009−3014.
(16) Lotero, E.; Liu, Y.; Lopez, D. E.; Suwannakarn, K.; Bruce, D. A.; Goodwin, J. G. Synthesis of Biodiesel via Acid Catalysis. *Ind. Eng. Chem. Res.* **2005**, *44*, 5353−5363.
(17) Meher, L. C.; Vidya Sagar, D.; Naik, S. N. Technical Aspects of Biodiesel Production by Transesterification - A Review. *Renewable Sustainable Energy Rev.* **2006**, 248−268.
(18) Sasidharan, M.; Kumar, R. Transesterification over Various Zeolites under Liquid-Phase Conditions. *J. Mol. Catal. A: Chem.* **2004**, *210*, 93−98.
(19) Peng, B. X.; Shu, Q.; Wang, J. F.; Wang, G. R.; Wang, D. Z.; Han, M. H. Biodiesel Production from Waste Oil Feedstocks by Solid Acid Catalysis. *Process Saf. Environ. Prot.* **2008**, *86*, 441−447.
(20) Kiss, A. A.; Dimian, A. C.; Rothenberg, G. Solid Acid Catalysts for Biodiesel Production - Towards Sustainable Energy. *Adv. Synth. Catal.* **2006**, *348*, 75−81.
(21) Furuta, S.; Matsuhashi, H.; Arata, K. Catalytic Action of Sulfated Tin Oxide for Etherification and Esterification in Comparison with Sulfated Zirconia. *Appl. Catal., A* **2004**, *269*, 187−191.
(22) Istadi, I.; Anggoro, D. D.; Buchori, L.; Rahmawati, D. A.; Intaningrum, D. Active Acid Catalyst of Sulphated Zinc Oxide for Transesterification of Soybean Oil with Methanol to Biodiesel. *Procedia Environ. Sci.* **2015**, *23*, 385−393.
(23) Zhang, G.; Xie, W. ZrMo oxides supported catalyst with hierarchical porous structure for cleaner and sustainable production of biodiesel using acidic oils as feedstocks. *J. Cleaner Prod.* **2023**, *384*, No. 135594.
(24) Lin, K.-S.; Mdlovu, N. V.; Chan, H.-Y.; Wu, K. C.-W.; Wu, J. C.-S.; Huang, Y.-T. Preparation and characterization of mesoporous polymer-based solid acid catalysts for biodiesel production via transesterification of palmitic oils. *Catal. Today* **2022**, *397-399*, 145−154.
(25) Narasimhan, M.; Chandrasekaran, M.; Govindasamy, S.; Aravamudhan, A. Heterogeneous nanocatalysts for sustainable biodiesel production: A review. *J. Environ. Chem. Eng.* **2021**, *9*, No. 104876.
(26) Madhuvilakku, R.; Piraman, S. Biodiesel synthesis by TiO2-ZnO mixed oxide nanocatalyst catalysed palm oil transesterification process. *Bioresour. Technol.* **2013**, *150*, 55−59.
(27) Saravanan, K.; Tyagi, B.; Shukla, R. S.; Bajaj, H. C. Solvent free synthesis of methyl palmitate over sulfated zirconia solid acid catalyst. *Fuel* **2016**, *165*, 298−305.
(28) Bahadoran, A.; Ramakrishna, S.; Oryani, B.; Al-Keridis, L. A.; Nodeh, H. R.; Rezania, S. Biodiesel production from waste cooking oil using heterogeneous nanocatalyst-based magnetic polyaniline decorated with cobalt oxide. *Fuel* **2022**, *319*, No. 123858.
(29) Qiu, T.; Guo, X.; Yang, J.; Zhou, L.; Li, L.; Wang, H.; Niu, Y. The synthesis of biodiesel from coconut oil using novel Brønsted acidic ionic liquid as green catalyst. *Chem. Eng. J.* **2016**, *296*, 71−78.
(30) Zhang, B.; Gao, M.; Tang, W.; Wang, X.; Wu, C.; Wang, Q.; Cheung, S. M.; Chen, X. Esterification efficiency improvement of carbon-based solid acid catalysts induced by biomass pretreatments: Intrinsic mechanism. *Energy* **2023**, *263*, No. 125606.
(31) Mao, Y.; Chen, J.; Guo, H.; Shao, Y.; Qian, L.; Yang, W. Sulfamic acid−modified zeolitic imidazolate framework (ZIF-90) with synergetic Lewis and Brønsted acid sites for microalgal biodiesel production. *Fuel* **2023**, *331*, No. 125795.
(32) Zhang, Q.; Lei, Y.; Li, L.; Lei, J.; Hu, M.; Deng, T.; Zhang, Y.; Ma, P. Construction of the novel PMA@Bi-MOF catalyst for effective fatty acid esterification. *Sustain. Chem. Pharm.* **2023**, *33*, No. 101038.
(33) Li, Y.; Zhu, K.; Jiang, Y.; Chen, L.; Zhang, H.; Li, H.; Yang, S. Biomass-derived hydrophobic metal-organic frameworks solid acid for green efficient catalytic esterification of oleic acid at low temperatures. *Fuel Process. Technol.* **2023**, *239*, No. 107558.
(34) Lia, H.; Chu, H.; Ma, X.; Wang, G.; Liu, F.; Guo, M.; Lu, W.; Zhou, S.; Yu, M. Efficient heterogeneous acid synthesis and stability enhancement of UiO-66impregnated with ammonium sulfate for biodiesel production. *Chem. Eng. J.* **2021**, *408*, No. 127277.
(35) Singh, A. K.; Fernando, S. D. Transesterifiation of soybean oil using heterogeneous catalysts. *Energy Fuels* **2008**, *22*, 2067−2069.
(36) Chakraborty, S.; Sirotiya, V.; Rai, A.; Varjani, S.; Vinayak, V. Catalyst in algal refinery: A way towards production of high-quality biofuel. *Sustain. Chem. Pharm.* **2023**, *33*, No. 101092.
(37) Jansen, J. C.; Creyghton, E. J.; Njo, S. L.; Van Koningsveld, H.; Van Bekkum, H. On the Remarkable Behaviour of Zeolite Beta in Acid Catalysis. *Catal. Today* **1997**, *38*, 205−212.
(38) Katkar, S. S.; Mohite, P. H.; Gadekar, L. S.; Arbad, B. R.; Lande, M. K. ZnO-Beta Zeolite: As an Effective and Reusable Heterogeneous Catalyst for the One-Pot Synthesis of Polyhydroquinolines. *Green Chem. Lett. Rev.* **2010**, *3*, 287−292.
(39) Penzien, J.; Abraham, A.; Van Bokhoven, J. A.; Jentys, A.; Müller, T. E.; Sievers, C.; Lercher, J. A. Generation and Characterization of Well-Defined Zn2+ Lewis Acid Sites in Ion Exchanged Zeolite BEA. *J. Phys. Chem. B* **2004**, *108*, 4116−4126.
(40) Camblor, M. A.; Corma, A.; Valencia, S. Characterization of Nanocrystalline Zeolite Beta. *Microporous Mesoporous Mater.* **1998**, *25*, 59−74.
(41) Borah, M. J.; Devi, A.; Borah, R.; Deka, D. Synthesis and Application of Co Doped ZnO as Heterogeneous Nanocatalyst for Biodiesel Production from Non-Edible Oil. *Renewable Energy* **2019**, *133*, 512−519.
(42) Beers, A. E. W.; Van Bokhoven, J. A.; De Lathouder, K. M.; Kapteijn, F.; Moulijn, J. A. Optimization of Zeolite Beta by Steaming and Acid Leaching for the Acylation of Anisole with Octanoic Acid: A Structure-Activity Relation. *J. Catal.* **2003**, *218*, 239−248.
(43) Reddy, M. M.; Kumar, M. A.; Swamy, P.; Naresh, M.; Srujana, K.; Satyanarayana, L.; Venugopal, A.; Narender, N. N-Alkylation of Amines with Alcohols over Nanosized Zeolite Beta. *Green Chem.* **2013**, *15*, 3474−3483.
(44) Ikuno, T.; Chaikittisilp, W.; Liu, Z.; Iida, T.; Yanaba, Y.; Yoshikawa, T.; Kohara, S.; Wakihara, T.; Okubo, T. Structure-Directing Behaviors of Tetraethylammonium Cations toward Zeolite Beta Revealed by the Evolution of Aluminosilicate Species Formed during the Crystallization Process. *J. Am. Chem. Soc.* **2015**, *137*, 14533−14544.
(45) Dzwigaj, S.; Janas, J.; Gurgul, J.; Socha, R. P.; Shishido, T.; Che, M. Do Cu(II) Ions Need Al Atoms in Their Environment to Make CuSiBEA Active in the SCR of NO by Ethanol or Propane? A Spectroscopy and Catalysis Study. *Appl. Catal., B* **2009**, *85*, 131−138.
(46) Singh, D.; Bhoi, R.; Ganesh, A.; Mahajani, S. Synthesis of Biodiesel from Vegetable Oil Using Supported Metal Oxide Catalysts. *Energy Fuels* **2014**, *28*, 2743−2753.
(47) Singh, D.; Patidar, P.; Ganesh, A.; Mahajani, S. Esterification of Oleic Acid with Glycerol in the Presence of Supported Zinc Oxide as Catalyst. *Ind. Eng. Chem. Res.* **2013**, *52*, 14776−14786.
(48) Kaningini, A. G.; Azizi, S.; Sintwa, N.; Mokalane, K.; Mohale, K. C.; Mudau, F. N.; Maaza, M. Effect of Optimized Precursor Concentration, Temperature, and Doping on Optical Properties of ZnO Nanoparticles Synthesized via a Green Route Using Bush Tea (Athrixia Phylicoides DC.) Leaf Extracts. *ACS Omega* **2022**, *7*, 31658−31666.
(49) Lee, H. J.; Kang, D.; Kim, E.; Suh, Y.; Kim, D.; Han, H.; Min, H. Production of $H_2$ -Free Carbon Monoxide from Formic Acid Dehydration: The Catalytic Role of Acid Sites in Sulfated Zirconia. *Nanomaterials* **2022**, *12*, 3036.


https://doi.org/10.1021/acsomega.3c01892
*ACS Omega* 2023, 8, 23720−23732

(50) Van Oers, C. J.; Stevens, W. J. J.; Bruijn, E.; Mertens, M.; Lebedev, O. I.; Van Tendeloo, G.; Meynen, V.; Cool, P. Formation of a Combined Micro- and Mesoporous Material Using Zeolite Beta Nanoparticles. *Microporous Mesoporous Mater.* **2009**, *120*, 29−34.
(51) Sahu, P.; Sakthivel, A. Zeolite- b Based Molecular Sieves: A Potential Catalyst for Esterification of Biomass Derived Model Compound Levulinic Acid. *Mater. Sci. Energy Technol.* **2021**, *4*, 307−316.
(52) Dzwigaj, S.; Massiani, P.; Davidson, A.; Che, M. Role of Silanol Groups in the Incorporation of V in $\beta$ Zeolite. *J. Mol. Catal. A: Chem.* **2000**, *155*, 169−182.
(53) Tielens, F.; Calatayud, M.; Dzwigaj, S.; Che, M. What Do Vanadium Framework Sites Look like in Redox Model Silicate Zeolites? *Microporous Mesoporous Mater.* **2009**, *119*, 137−143.
(54) Emeis, C. A. Determination of integrated molar extinction coefficients for infrared absorption bands of pyridine adsorbed on solid acid catalysts. *J Catal.* **1993**, *141*, 347−354.
(55) Thommes, M. Physical Adsorption Characterization of Nanoporous Materials. *Chem. Ing. Tech.* **2010**, *82*, 1059−1073.
(56) Schmidt, S. A.; Kumar, N.; Shchukarev, A.; Eränen, K.; Mikkola, J. P.; Murzin, D. Y.; Salmi, T. Preparation and Characterization of Neat and ZnCl2 Modified Zeolites and Alumina for Methyl Chloride Synthesis. *Appl. Catal., A* **2013**, *468*, 120−134.
(57) Tariq, M.; Ali, S.; Ahmad, F.; Ahmad, M.; Zafar, M.; Khalid, N.; Khan, M. A. Identification, FT-IR, NMR (1H and 13C) and GC/MS Studies of Fatty Acid Methyl Esters in Biodiesel from Rocket Seed Oil. *Fuel Process. Technol.* **2011**, *92*, 336−341.
(58) Monteiro, M. R.; Ambrozin, A. R. P.; Lião, L. M.; Ferreira, A. G. Determination of Biodiesel Blend Levels in Different Diesel Samples by 1H NMR. *Fuel* **2009**, *88*, 691−696.
(59) Xie, W.; Peng, H.; Chen, L. Transesterification of Soybean Oil Catalyzed by Potassium Loaded on Alumina as a Solid-Base Catalyst. *Appl. Catal., A* **2006**, *300*, 67−74.
(60) Mansir, N.; Teo, S. H.; Rashid, U.; Taufiq-Yap, Y. H. Efficient Waste Gallus Domesticus Shell Derived Calcium-Based Catalyst for Biodiesel Production. *Fuel* **2018**, *211*, 67−75.
(61) Xie, W.; Huang, X. Synthesis of Biodiesel from Soybean Oil Using Heterogeneous KF/ZnO Catalyst. *Catal. Lett.* **2006**, *107*, 53−59.
(62) Feyzi, M.; Shahbazi, E. Catalytic Performance and Characterization of Cs-Ca/SiO2-TiO2 Nanocatalysts for Biodiesel Production. *J. Mol. Catal. A: Chem.* **2015**, *404*, 131−138.
(63) Abu-Jrai, A. M.; Jamil, F.; Al-Muhtaseb, A. H.; Baawain, M.; Al-Haj, L.; Al-Hinai, M.; Al-Abri, M.; Rafiq, S. Valorization of Waste Date Pits Biomass for Biodiesel Production in Presence of Green Carbon Catalyst. *Energy Convers. Manage.* **2017**, *135*, 236−243.
(64) Kaur, N.; Ali, A. Preparation and Application of Ce/ZrO2-TiO2/SO42- as Solid Catalyst for the Esterification of Fatty Acids. *Renewable Energy* **2015**, *81*, 421−431.
(65) Sahani, S.; Sharma, Y. C. Economically Viable Production of Biodiesel Using a Novel Heterogeneous Catalyst: Kinetic and Thermodynamic Investigations. *Energy Convers. Manage.* **2018**, *171*, 969−983.
(66) Zhang, Q.; Ling, D.; Lei, D.; Wang, J.; Liu, X.; Zhang, Y. Green and Facile Synthesis of Metal-Organic Framework Cu-BTC-Supported Sn (II) -Substituted Keggin Heteropoly Composites as an Esterification Nanocatalyst for Biodiesel Production. *Front. Chem.* **2020**, *8*, 129.
(67) Patel, A.; Brahmkhatri, V. Kinetic Study of Oleic Acid Esterification over 12-Tungstophosphoric Acid Catalyst Anchored to Different Mesoporous Silica Supports. *Fuel Process. Technol.* **2013**, *113*, 141−149.
(68) Freedman, B.; Pryde, E. H.; Mounts, T. L. Variables Affecting the Yields of Fatty Esters from Transesterified Vegetable Oils. *J. Am. Oil Chem. Soc.* **1984**, *61*, 1638−1643.
(69) Barakos, N.; Pasias, S.; Papayannakos, N. Transesterification of Triglycerides in High and Low Quality Oil Feeds over an HT2 Hydrotalcite Catalyst. *Bioresour. Technol.* **2008**, *99*, 5037−5042.
(70) Yan, S.; Salley, S. O.; Simon Ng, K. Y. Simultaneous Transesterification and Esterification of Unrefined or Waste Oils over ZnO-La2O3 Catalysts. *Appl. Catal., A* **2009**, *353*, 203−212.
(71) Jacobson, K.; Gopinath, R.; Meher, L. C.; Dalai, A. K. Solid Acid Catalyzed Biodiesel Production from Waste Cooking Oil. *Appl. Catal., B* **2008**, *85*, 86−91.
(72) Kulkarni, M. G.; Gopinath, R.; Meher, L. C.; Dalai, A. K. Solid Acid Catalyzed Biodiesel Production by Simultaneous Esterification and Transesterification. *Green Chem.* **2006**, *8*, 1056−1062.
(73) Vieira, S. S.; Magriotis, Z. M.; Graça, I.; Fernandes, A.; Ribeiro, M. F.; Lopes, J. M. F. M.; Coelho, S. M.; Santos, N. A. V.; Saczk, A. A. Production of Biodiesel Using HZSM-5 Zeolites Modified with Citric Acid and SO42−/La2O3. *Catal. Today* **2017**, *279*, 267−273.
(74) Du, L.; Ding, S.; Li, Z.; Lv, E.; Lu, J.; Ding, J. Transesterification of Castor Oil to Biodiesel Using NaY Zeolite-Supported La2O3 Catalysts. *Energy Convers. Manage.* **2018**, *173*, 728−734.
(75) Lawan, I.; Garba, Z. N.; Zhou, W.; Zhang, M.; Yuan, Z. Synergies between the Microwave Reactor and CaO/Zeolite Catalyst in Waste Lard Biodiesel Production. *Renewable Energy* **2020**, *145*, 2550−2560.


https://doi.org/10.1021/acsomega.3c01892
*ACS Omega* 2023, 8, 23720−23732